Hindawi
Journal of Engineering
Volume 2023, Article ID 6630739, 9 pages
https://doi.org/10.1155/2023/6630739

Research Article

Energy Calibration and Inverse-Square Law of Radiation in Gamma-Ray Measurement Using a Scintillation Detector for Laboratory Experiments

Shiori Iida and Wei-Guo Jin

Department of Physics, Faculty of Science, Toho University, Funabashi-shi, Chiba 274-8510, Japan

Correspondence should be addressed to Wei-Guo Jin; jin@ph.sci.toho-u.ac.jp

Received 21 March 2023; Revised 18 September 2023; Accepted 8 November 2023; Published 18 November 2023

Academic Editor: Michela Dalle Mura

Over the past two years, third-year undergraduate students from Toho University's Department of Physics conducted laboratory experiments on gamma-ray measurement using a scintillation detector. Approximately, 30 experimental data points were collected and subsequently analyzed. The analysis focused on the energy calibration method and the inverse-square law of radiation. Results revealed that employing quadratic or cubic function fits for energy calibration yielded more than twice the accuracy compared to the conventional linear function fit. Regarding the deviation from the inverse-square law of radiation, a correction method utilizing a correction parameter was compared with a power function fit method. The discussion encompassed the correction parameter and the exponent of the power function.

1. Introduction

Gamma-ray measurement holds significance in nuclear physics as it pertains to fundamental physics [1–3] and radiation measurement [4–9]. The Fukushima Daiichi Nuclear Power Plant accident, triggered by the Great East Japan Earthquake of March 11, 2011, led to the release of radioactive materials. Consequently, a substantial area, centered on Fukushima Prefecture, remains contaminated. This incident has heightened the interest in the radiation's fundamental knowledge and measurement technology [10–13]. Measurement of the relationship between gamma-ray intensity and distance is essential for radiation protection, while energy spectrum measurement is vital for radiation object identification [14].

The scintillation detector presents several advantageous characteristics, including affordability, stability, and user-friendliness [15]. It serves as a fundamental instrument for gamma-ray measurement and finds applications in laboratory experiments across numerous universities [16–22]. Through these experiments, students not only acquire gamma-ray measurement techniques but also gain insights into the interaction between gamma-ray and matter.

Toho University's Department of Physics has conducted laboratory experiments on gamma-ray measurement using the scintillation detector for several years, specifically targeting third-year undergraduates [23]. Since these experiments are conducted annually, it is suitable for the radioactive source [24, 25] to possess a half-life of several years or more. Accordingly, Toho University employs three radioactive sources: ^{137}Cs, ^{60}Co, and ^{22}Na. Within the laboratory experiment, measurements of gamma-ray spectrum and intensity with distance were conducted. Spectral measurements [26] involved obtaining energies of positron annihilation peaks from ^{22}Na through energy calibration using a linear function fit. The photopeaks at 662 keV of ^{137}Cs, 1173 and 1333 keV of ^{60}Co, and 1275 keV of ^{22}Na were utilized [7, 8, 27]. The efficiency of the NaI (Tl) detector has been extensively studied for various radioactive sources by the Alexandria University research group [28–37]. However, the experimental positron annihilation peak energy of ^{22}Na consistently exhibited a deviation of more than 10% from the

theoretical value. In the intensity measurement with distance, the deviation from the inverse-square law of radiation intensity [38–40] was analyzed by introducing a correction parameter. However, the utilization of this correction parameter complicated students' understanding of the inverse-square law of radiation. Furthermore, neither the comprehension of the correction parameter itself nor the recommended value for it is currently known.

This study aims to collect approximately 30 experimental data points obtained by students during laboratory experiments conducted in the third-year of Toho University's Department of Physics. The collected data will be analyzed to assess the deviation in conventional energy calibration and the deviation from the inverse-square law of radiation. Improved fits for energy calibration and recommended parameters for the inverse-square law of radiation are examined and discussed.

2. Experimental Setup and Methods

The experiments utilized three radioactive point sources: ^{137}Cs, ^{60}Co, and ^{22}Na. Figure 1(a) illustrates a typical sealed radioactive point source of ^{60}Co, including its container. The scintillation detector used (OKEN SP-20) is shown in Figure 1(b), which consists of a 2-inch NaI (Tl) scintillator, a photomultiplier tube, and a preamplifier. Figure 1(c) depicts the arrangement during measurements, with the source and scintillation detector positioned on a wooden straight rail within a box, ensuring they remain in line and facilitating accurate distance measurements.

The complete experimental setup is presented in Figure 1(d). The photomultiplier tube received a voltage of 500–700 V from a high voltage supply (OKEN 714-1C). The output from the scintillation detector was amplified using a linear amplifier (OKEN 704-4B). The radioactivity intensity, or gamma-ray count, was measured with a scaler (OKEN 711-6), while the gamma-ray spectrum was measured using a multichannel analyzer (MCA) (HOSHIN ELECTRONICS HE1442).

Figure 2 displays the decay schemes of the three sources [7, 8, 27]. ^{137}Cs has a half-life of 30.0 years and emits a 662 keV gamma-ray through β^- decay. ^{60}Co has a half-life of 5.27 years and emits two gamma rays of 1173 and 1333 keV through β^- decay. ^{22}Na has a half-life of 2.60 years and emits a 1275 keV gamma-ray through β^+ decay. The characteristics and long half-lives of the three sources of ^{137}Cs, ^{60}Co, and ^{22}Na render them highly suitable for laboratory experiments. The initial intensities used for these sources in this experiment were 3.7×10^5 Bq.

3. Results and Discussion

3.1. Energy Calibration. Figure 3 presents typical energy spectra of ^{137}Cs, ^{60}Co, and ^{22}Na, as measured by a student. In the ^{137}Cs spectrum, the full width at half maximum of the 662 keV photopeak is approximately 80 keV. This resolution suffices for laboratory experiments, as the double peaks of ^{60}Co are clearly distinguished. The backscatter peak was frequently observed in the ^{137}Cs spectrum but rarely in the ^{60}Co and ^{22}Na spectra.

During laboratory experiments, the Gaussian distribution photopeaks at 662 keV of ^{137}Cs, 1173 and 1333 keV of ^{60}Co, and 1275 keV of ^{22}Na were employed for energy calibration of the MCA channels. A least-squares fit with a linear function was used to establish the relationship between channel and energy by measuring the central channel numbers of the aforementioned four photopeaks. Figure 4 displays a typical linear function fit, revealing a substantial intercept. By using the fitted linear function, the experimental energy value E^e_{ex} of the positron annihilation peak from ^{22}Na was determined. However, the obtained experimental value E^e_{ex} consistently deviated by more than 10% from the theoretical value $E^e_{\mathrm{th}} = 0.511$ MeV.

Considering that the MCA offset is typically adjusted to pass through the origin, this study examined the deviation of the experimental value E^e_{ex} by fitting the data using a linear function, a quadratic function, and a cubic function, while considering the origin. Figure 4 illustrates the typical lines resulting from least-squares fits to the experimental data. The conventional linear function fit without considering the origin (L1) is compared with the linear function fit considering the origin (L10), the quadratic function fit considering the origin (L20), and the cubic function fit considering the origin (L30).

The energy calibration line was evaluated using the gamma-ray photopeak from ^{22}Na positron annihilation, and the energy value E^e_{ex} was obtained from the central channel number of the peak using the calibration line. By comparing the experimental value E^e_{ex} with the theoretical value E^e_{th}, a relative deviation S was calculated using the following formula:

$$S = \frac{E^e_{\mathrm{ex}} - E^e_{\mathrm{th}}}{E^e_{\mathrm{th}}}. \quad (1)$$

All three functions, along with the conventional method shown in Figure 4, were fitted to the data collected by third-year students over the past two years, and the relative deviation S was determined. Figure 5 presents the distribution of S for the collected data. The range of S is observed to be 9%–13% for L1 and L10, and 2%–6% for L20 and L30. The average values of S are as follows: $S = 10.5$ (2)% for L1, $S = 11.6$ (2)% for L10, $S = 4.7$ (2)% for L20, and $S = 3.6$ (3)% for L30. It is noteworthy that the quadratic function (L20) and cubic function (L30) fits yielded more than a twofold improvement in the relative deviation.

3.2. Inverse-Square Law of Radiation. In the experiment, counts were recorded by varying the distance R from the detector to the radioactive source, ranging from 2 to 48 cm. By subtracting the background counts and considering only counts from the radioactive source, the count rate K was determined. Figure 6 presents typical data showing the count rate K as a function of distance R, as measured by the students. The experimental data were fitted with an inverse-square function (equation (2)) that includes a constant term K_0:

$$K = \frac{K_0}{R^2}. \quad (2)$$

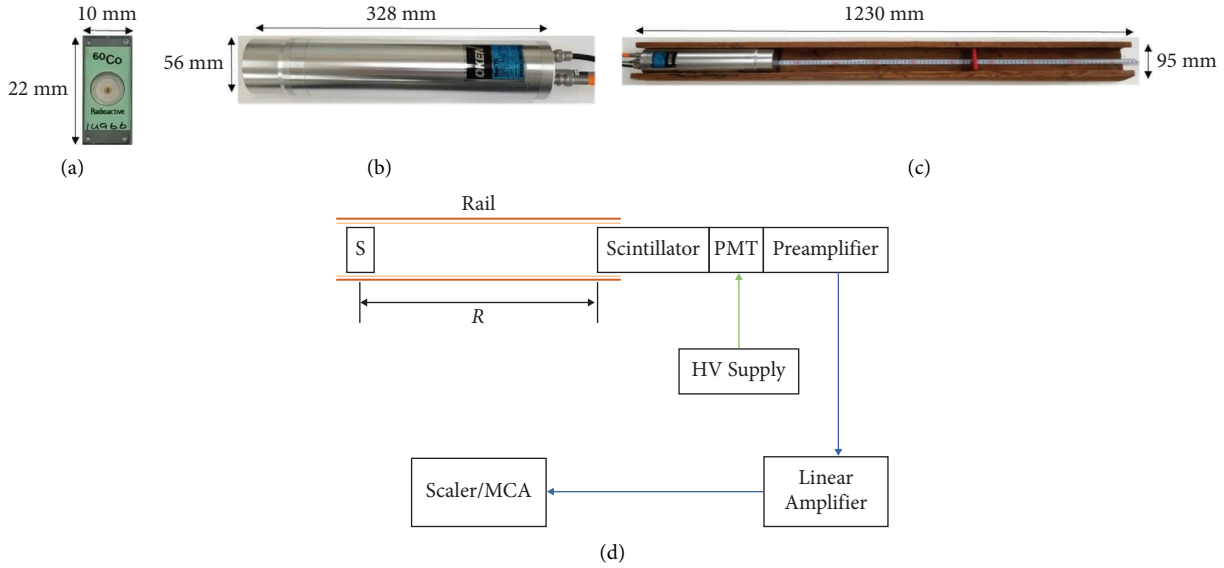

Figure 1: Sealed radioactive point source of ^{60}Co (a), the scintillation detector (b), the arrangement of the source and the scintillation detector (c), and the entire experimental setup (d). *S* denotes source, PMT denotes photomultiplier tube, HV denotes high voltage, and MCA denotes multichannel analyzer.

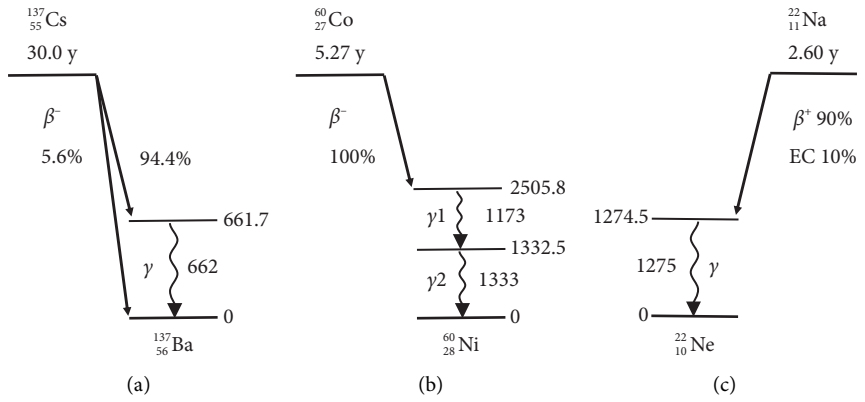

Figure 2: Decay schemes of radioactive sources ^{137}Cs (a), ^{60}Co (b), and ^{22}Na (c). Energy unit is keV.

Two separate fittings were performed: one using data from 2 to 48 cm and another using data from 12 to 48 cm. The fitted lines are plotted in Figure 6. It is evident from Figure 6 that the data from 2 to 48 cm deviate significantly from the inverse-square function. However, the data from 12 to 48 cm exhibit a closer alignment with the inverse-square function, although some deviation remains. Similar trends are observed for ^{137}Cs and ^{60}Co sources. This suggests that gamma-ray intensity does not strictly follow the inverse-square law within a distance of 10 cm, and particularly at short distances of a few cm, it deviates considerably from the inverse-square law.

Dead time of the detector may be one of the reasons for this deviation from the inverse-square law in Figure 6. Influence of dead time will become strong with loss of count for strong count rate. ^{137}Cs and ^{60}Co have a large difference of count rate: count rate of ^{137}Cs is about one order of magnitude larger than that of ^{60}Co. Therefore, the influence of dead time, i.e., possibly induced deviation from the inverse-square law, should be strong for ^{137}Cs. Since the dead time in our detector has an order of magnitude of μs, the influence on count, i.e., loss of count, can be neglected for present lower count rate (~10^3 cps) as shown in Figure 6. For ^{60}Co, the coincidence summing effect due to the cascade gamma-rays of 1173 and 1333 keV may be another reason for the deviation from the inverse-square law. The coincidence summing effect is dependent on the detector type and geometry and becomes strong at close distance between the source and detector. However, since the total counts from the source, rather than the photopeak, were measured in this experiment using a scaler influence from the coincidence summing effect should be greatly reduced.

To check the influence of the dead time and coincidence summing effect on deviation from the inverse-square law, the relative deviation K_D of the experimental count rate (K_{exp}) from the fitted line of equation (2) (K_{fit}) is defined as follows:

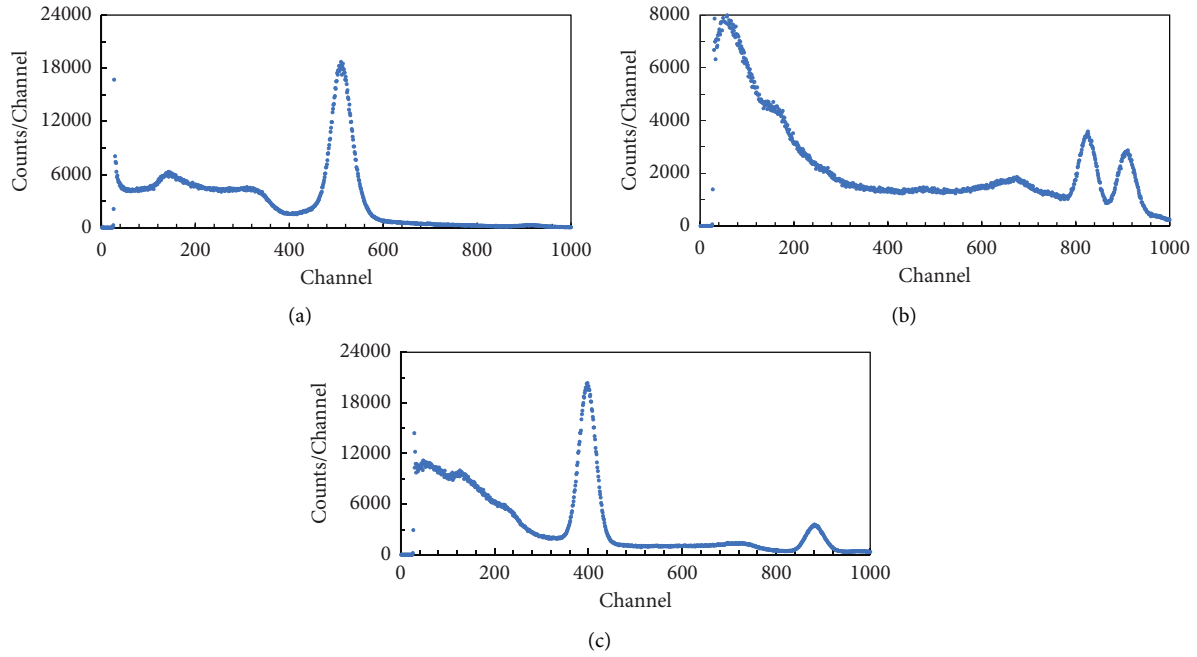

Figure 3: Typical measured gamma-ray energy spectra of ^{137}Cs (a), ^{60}Co (b), and ^{22}Na (c). All sources were placed at a distance of 2 cm from the detector. (a) Measured for 10 min and (b) and (c) measured for 120 min.

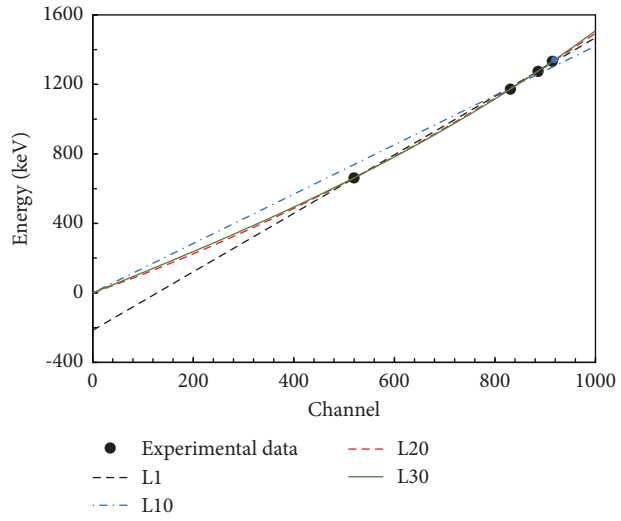

Figure 4: Typical experimental data of energy versus channel number measured for the photopeaks of 662 keV of ^{137}Cs, 1173 and 1333 keV of ^{60}Co, and 1275 keV of ^{22}Na. Experimental errors of the channel are within the symbols. Lines are the least-squares fits to the data. L1 denotes the conventional linear function fit without considering the origin, L10 denotes the linear function fit considering the origin, L20 denotes the quadratic function fit considering the origin, and L30 denotes the cubic function fit considering the origin.

$$K_{\mathrm{D}} = \frac{K_{\mathrm{fit}} - K_{\mathrm{exp}}}{K_{\mathrm{exp}}}. \quad (3)$$

Results of K_D calculated from Figure 6 for experimental data of K from 2 to 48 cm are shown in Figure 7. It can be seen from Figure 7 that K_D of ^{137}Cs agrees well with that of ^{60}Co with a same trend. This shows that influence of the dead time and coincidence summing effect on the deviation from the inverse-square law is negligibly small. Therefore, detailed corrections of the dead time and coincidence summing effect were not performed in this experiment. These possible influences, very weak as shown in Figure 7, can be included in the correction method using a parameter shown as follows.

The main reason for the deviation from the inverse-square law is considered to be from the measured distance. The measured distance R from the center of the source to the front surface of the detector differs from the actual distance $(R + a)$ from the emitted point of gamma rays to the measured point. Here, a mainly accounts for this difference between the measured and actual distances. To correct the

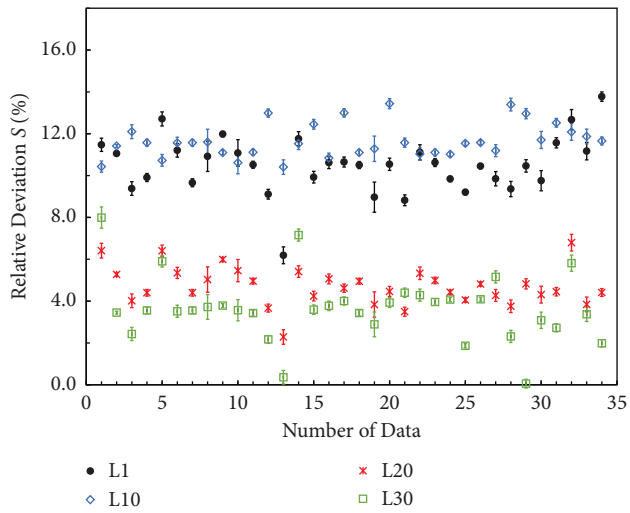

FIGURE 5: Comparison of the relative deviation S for the L1, L10, L20, and L30 fits. Error bar shows the standard deviation of measurements.

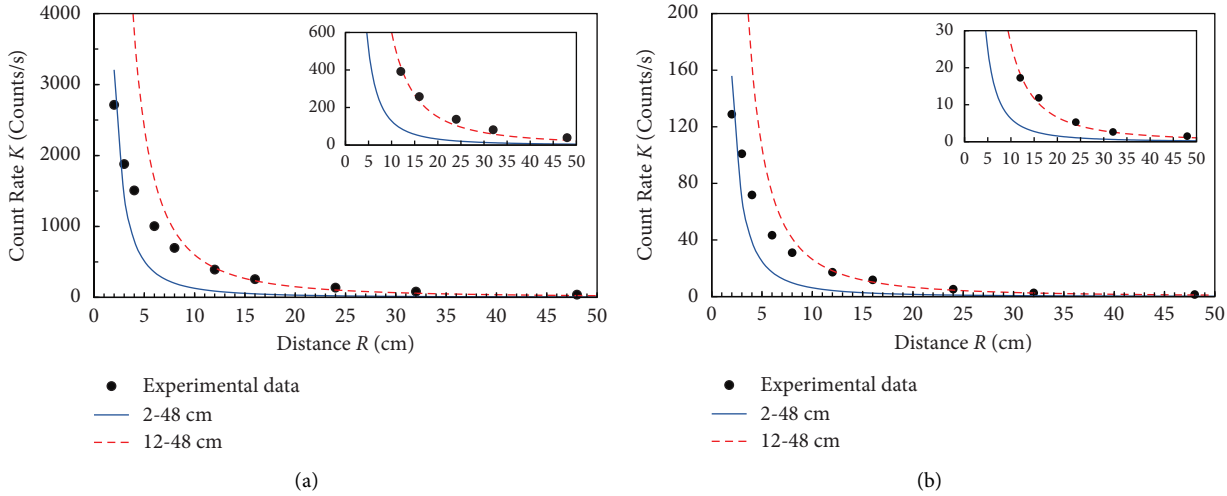

FIGURE 6: Typical experimental data on the count rate K versus distance R. Experimental statistical errors of K are within the symbols. Lines are the least-squares fits with the inverse-square function of equation (2) to data from 2 to 48 cm and data from 12 to 48 cm for ^{137}Cs (a) and ^{60}Co (b). The insert is the expanded figure showing the fitting of the data from 12 to 48 cm.

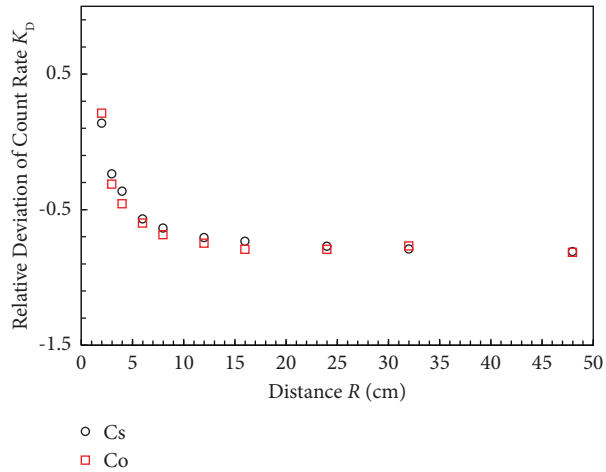

FIGURE 7: Relative deviation K_D of the experimental count rate (K_{exp}) from the fitted line of equation (2) (K_{fit}) calculated from Figure 6 for experimental data of K from 2 to 48 cm for ^{137}Cs and ^{60}Co.

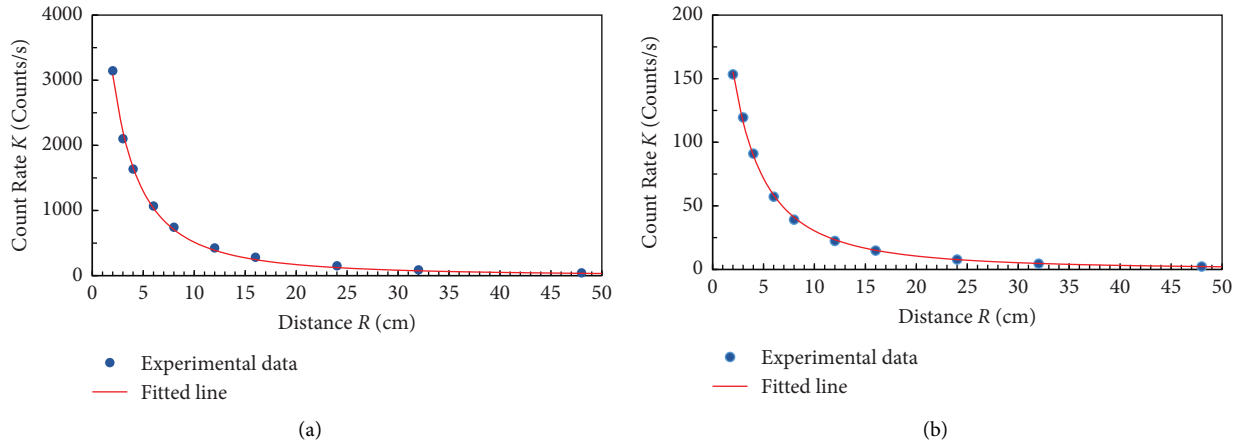

FIGURE 8: Typical lines of the least-squares fit with the modified inverse-square function of equation (4) to experimental data of K from 2 to 48 cm for ^{137}Cs (a) and ^{60}Co (b). Experimental statistical errors of K are within the symbols.

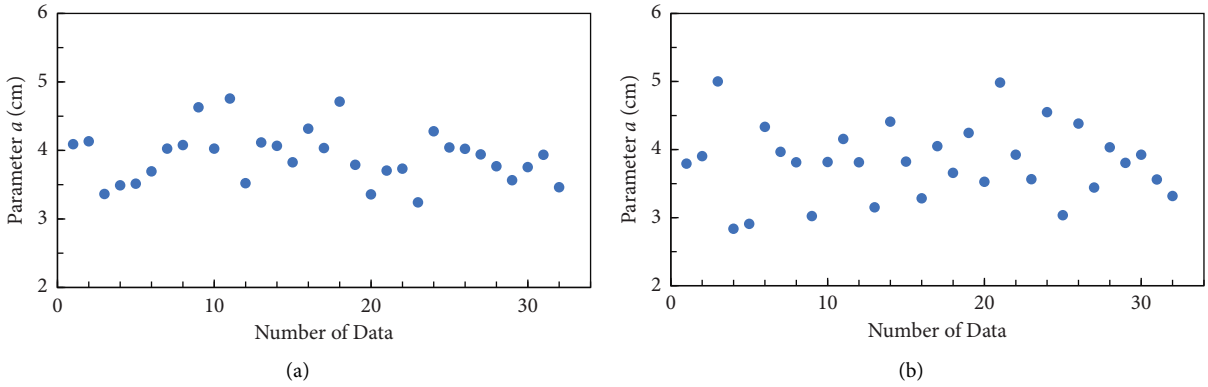

FIGURE 9: Distribution of the correction parameter a for ^{137}Cs (a) and ^{60}Co (b).

deviation from the inverse-square law in laboratory experiments, a correction parameter a was introduced, and the data were fitted with a modified inverse-square function (equation (4)) that includes a constant term K_1:

$$K = \frac{K_1}{(R+a)^2}. \tag{4}$$

Figure 8 illustrates a typical example of fitting the modified inverse-square function to the data from 2 to 48 cm, demonstrating suitable agreement between the fitted function and the experimental data for both ^{137}Cs and ^{60}Co sources. The recommended values for the correction parameter a were obtained by collecting data taken by students over the past two years, from 2 to 48 cm. Figure 9 presents the distribution of the correction parameter a. As observed, the values of a for ^{137}Cs and ^{60}Co sources are distributed in the range of 3–5 cm. The average values are determined as follows:

$$\begin{aligned} a &= 3.91\,(7)\ \text{cm for}^{137}\text{Cs}, \\ a &= 3.81\,(9)\ \text{cm for}^{60}\text{Co}. \end{aligned} \tag{5}$$

The obtained values of a for ^{137}Cs and ^{60}Co sources agree within experimental uncertainties, indicating that the effect of the difference in sources on the parameter a is negligibly small. Additionally, the obtained a values of approximately 4 cm are reasonable for the 2-inch NaI (Tl) scintillator used in the experiment.

In this study, a direct fitting approach was applied using a power function (equation (5)) without incorporating the correction parameter.

$$K = \frac{K_2}{R^b}. \tag{6}$$

Here, b is the exponent of the power function and K_2 is a constant. Figure 10 displays typical results of the least-squares fits using the power function for the ^{137}Cs source. Figure 10(a) illustrates the fit of data from 2 to 48 cm, Figure 10(b) shows the fit of data from 6 to 48 cm, and Figure 10(c) presents the fit of data from 12 to 48 cm. It is evident from Figures 10(a)–10(c) that the power function provides a good fit to the data. The analysis reveals that the exponent b of the power function increases as the distance R increases. By utilizing the data from 2 to 48 cm, the values of the exponent b were obtained through fits of the power function to the collected data from the students. Figure 11 depicts the distribution of the exponent b. For both ^{137}Cs and ^{60}Co sources, the exponent b is distributed between 1.30 and 1.55. The average values are determined as follows:

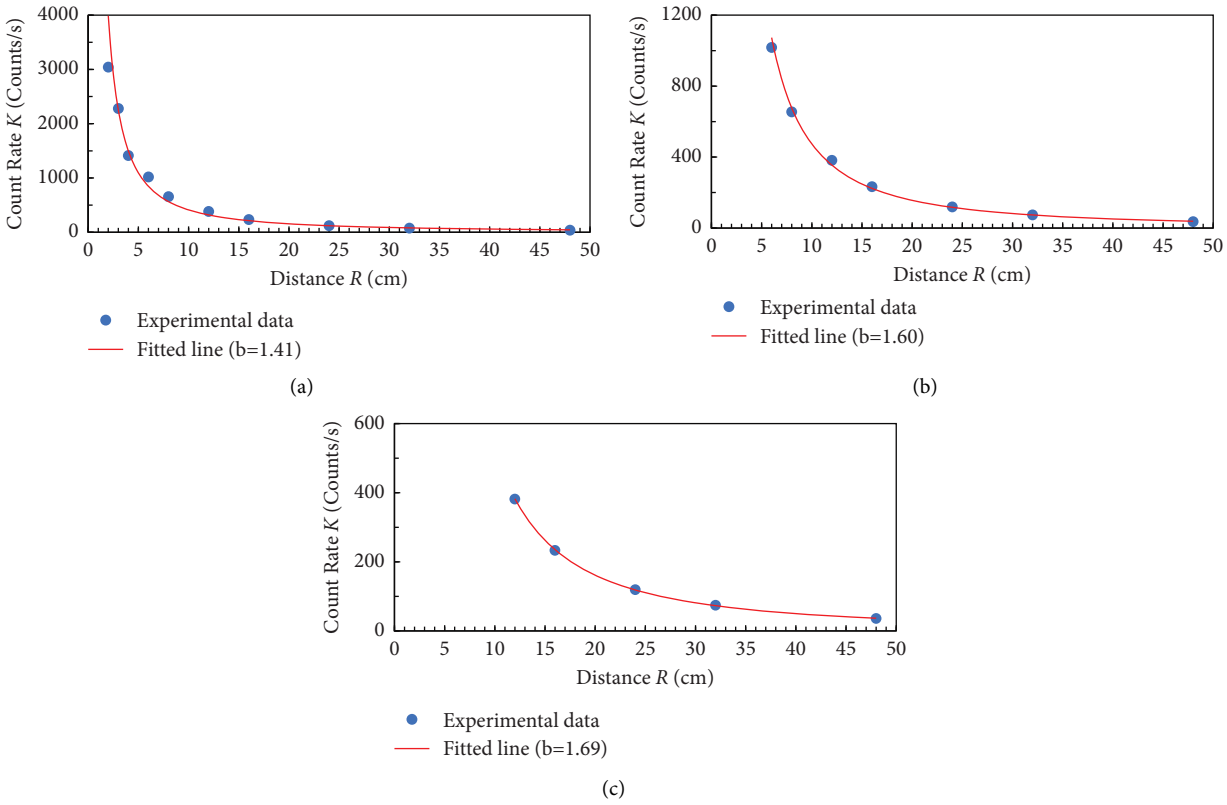

FIGURE 10: Typical lines of the least-squares fit with the power function of equation (5) to the experimental data of K for ^{137}Cs from 2 to 48 cm (a), from 6 to 48 cm (b), from 12 to 48 cm (c). Experimental statistical errors of K are within the symbols.

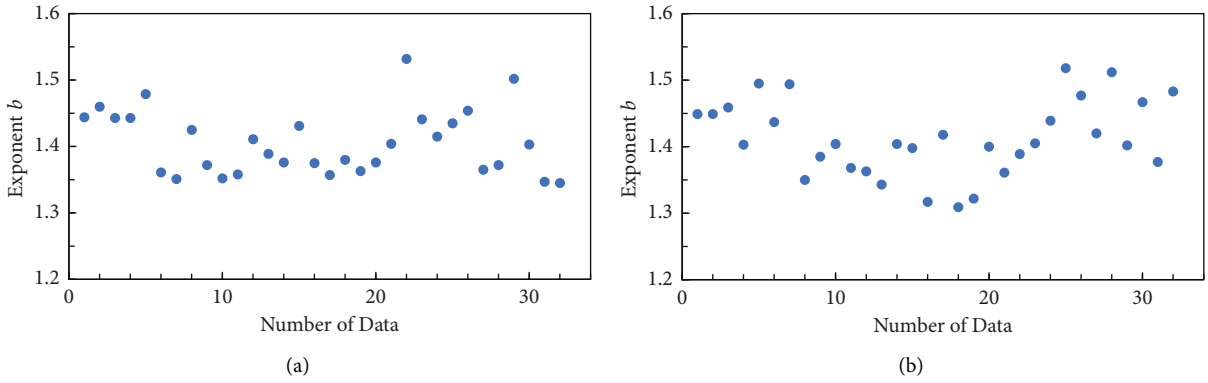

FIGURE 11: Distribution of the exponent b for ^{137}Cs (a) and ^{60}Co (b).

$$b = 1.405\,(9)\ \text{for}^{137}\text{Cs},$$
$$b = 1.413\,(10)\ \text{for}^{60}\text{Co}. \tag{7}$$

It is notable that the obtained values of b for ^{137}Cs and ^{60}Co agree within experimental uncertainties. This suggests that the exponent b, similar to the correction parameter a, is independent of the radioactive source.

4. Conclusions

In this study, the focus was on investigating energy calibration and the inverse-square law in gamma-ray measurements using data collected by students in laboratory experiments. Energy calibration was examined by comparing different fitting functions for the gamma-ray photopeak of ^{22}Na positron annihilation. The conventional linear function fit was compared with quadratic and cubic function fits. It was observed that both the quadratic and cubic function fits significantly improved the relative deviation between the experimental and theoretical values of the ^{22}Na positron annihilation peak compared with the linear function fit. However, there was no a substantial difference between the quadratic and cubic function fits. Regarding the inverse-square law of radiation, a large deviation was observed in the experimental data, with the deviation increasing as the distance decreased. To correct this deviation, a correction

parameter was introduced. The correction parameter allowed for a better fit of the experimental data to the inverse-square law. The distribution of the correction parameter was obtained from the student data, and the recommended value was provided based on the mean value. Furthermore, it was found that the experimental data could be well-fitted by directly applying a power function without using the correction parameter. The power function fitting provided an appropriate representation of the data without the need for additional corrections. The distribution of the power function exponent was obtained from the student data, and the recommended value was provided based on the mean value. Overall, this study demonstrated the importance of energy calibration and the challenges associated with the inverse-square law in gamma-ray measurements. The use of alternative fitting functions and the introduction of correction parameters or direct power function fits can significantly improve the accuracy and reliability of the measurements.

Data Availability

The data used to support the findings of this study are available upon request from the corresponding author.

Conflicts of Interest

The authors declare that there are no conflicts of interest regarding the publication of this paper.

Acknowledgments

This work was financially supported by Toho University.

References

[1] S. Ghosh, S. Dutta, N. K. Mondal, and S. Saha, "Measurements of gamma ray, cosmic muon and residual neutron background fluxes for rare event search experiments at an underground laboratory," *Astroparticle Physics*, vol. 139, Article ID 102700, 2022.

[2] I. G. Mitrofanov, M. L. Litvak, A. B. Sanin et al., "Laboratory demonstration of space gamma-ray spectroscopy experiment with tags of galactic cosmic rays for testing different types of martian regolith," *Nuclear Instruments and Methods in Physics Research Section A: Accelerators, Spectrometers, Detectors and Associated Equipment*, vol. 1028, Article ID 166364, 2022.

[3] S. Ghosh, S. Dutta, N. K. Mondal, and S. Saha, "Measurements and simulation of background radiation for rare event search experiments at an underground laboratory," *Journal of Physics: Conference Series*, vol. 2156, no. 1, Article ID 012168, 2021.

[4] M. Tzortzis, H. Tsertos, S. Christofides, and G. Christodoulides, "Gamma-ray measurements of naturally occurring radioactive samples from Cyprus characteristic geological rocks," *Radiation Measurements*, vol. 37, no. 3, pp. 221–229, 2003.

[5] A. Sakoda, H. Tanaka, and Y. Ishimori, "One-year measurements of gamma-ray background using a high-purity germanium detector," *Japanese Journal of Health Physics*, vol. 51, no. 4, pp. 245–250, 2016.

[6] D. Malczewski, J. Kisiel, and J. Dorda, "Gamma background measurements in the laboratoire souterrain de Modane," *Journal of Radioanalytical and Nuclear Chemistry*, vol. 292, no. 2, pp. 751–756, 2012.

[7] G. F. Knoll, *Radiation Detection And Measurement*, John Wiley & Sons, Hoboken, New Jersey, Third Edition, 2000.

[8] N. Tsoulfanidis, *Measurement and Detection of Radiation*, Taylor & Francis, Oxfordshire, England, Second Edition, 1995.

[9] L. Cerrito, Radiation and Detectors, *Introduction to the Physics of Radiation and Detection Devices*, Springer, Berlin, Heidelberg, 2017.

[10] T. Uemura and K. Yamaguchi, "Estimation of radiation source distribution using machine learning with γ ray energy spectra," *Journal of Advanced Simulation in Science and Engineering*, vol. 7, no. 1, pp. 71–81, 2020.

[11] K. Okada, T. Tadokoro, Y. Ueno et al., "Development of a gamma camera to image radiation fields," *Progress in Nuclear Science and Technology*, vol. 4, pp. 14–17, 2014.

[12] K. Sato, H. Murakami, and Y. Takashita, "Influence of counting loss on the inverse-square law of radiation," *Bulletin of Tokyo Gakugei University. Natural Sciences*, vol. 69, pp. 157–163, 2017.

[13] S. Yoshimoto, M. Imaizumi, S. Ishida, C. Ogura, and S. Okushima, "Analytical procedure for counting radiocesium peaks of gamma-ray spectra from in-situ measurements with NaI(Tl) scintillation spectrometers," *Technical Report of the National Institute for Rural Engineering*, vol. 214, pp. 175–196, 2013.

[14] J. E. Martin, *Physics for Radiation Protection*, Wiley VCH, Weinheim, Germany, 2013.

[15] T. Yanagida, "Inorganic scintillating materials and scintillation detectors," *Proceedings of the Japan Academy. Series B*, vol. 94, no. 2, pp. 75–97, 2018.

[16] R. M. Anjos, A. Facure, E. L. N. Lima et al., "Radioactivity teaching: environmental consequences of the radiological accident in goiânia (Brazil)," *American Journal of Physics*, vol. 69, no. 3, pp. 377–381, 2001.

[17] D.-M. Mei, C. Zhang, K. Thomas, and F. Gray, "Early results on radioactive background characterization for sanford laboratory and DUSEL experiments," *Astroparticle Physics*, vol. 34, no. 1, pp. 33–39, 2010.

[18] E. Adamides, S. K. Koutroubas, N. Moshonas, and K. Yiasemides, "Gamma ray attenuation measurements as a laboratory experiment: some remarks," *Physics Education*, vol. 46, no. 4, pp. 398–402, 2011.

[19] P. B. Siegel, "Gamma spectroscopy of environmental samples," *American Journal of Physics*, vol. 81, no. 5, pp. 381–388, 2013.

[20] D. Al-Azmi, N. Karunakara, and A. O. Mustapha, "Teaching about natural background radiation," *Physics Education*, vol. 48, no. 4, pp. 506–511, 2013.

[21] M. Pilakouta, A. Savidou, and S. Vasileiadou, "A laboratory activity for teaching natural radioactivity," *European Journal of Physics*, vol. 38, no. 1, Article ID 015801, 2017.

[22] J. Wen, X. Long, X. Zheng et al., "GRID: a student project to monitor the transient gamma-ray sky in the multi-messenger astronomy era," *Experimental Astronomy*, vol. 48, no. 1, pp. 77–95, 2019.

[23] P. Laboratory III, *Department of Physics*, Toho University, Funabashi, Japan, 2022.

[24] D. Al-Azmi, A. O. Mustapha, and N. Karunakara, "Radon adsorbed in activated charcoal—a simple and safe radiation

source for teaching practical radioactivity in schools and colleges," *Physics Education*, vol. 47, no. 4, pp. 471–475, 2012.
[25] P. Xu, C. Fu, Z.-Y. Tan, X.-F. Cai, and J. Qin, "Robust radioactive sources research method using possibility particle filter," *AIP Advances*, vol. 11, no. 8, Article ID 085308, 2021.
[26] M. Alamaniotis, J. Mattingly, and L. H. Tsoukalas, "Kernel-based machine learning for background estimation of NaI low-count gamma-ray spectra," *IEEE Transactions on Nuclear Science*, vol. 60, no. 3, pp. 2209–2221, 2013.
[27] S. Y. F. Chu, L. P. Ekström, and R. B. Firestone, "The Lund/LBNL Nuclear Data Search," 1999, http://nucleardata.nuclear.lu.se/toi/.
[28] A. M. El-Khatib, M. M. Gouda, M. S. Badawi, S. S. Nafee, and E. A. El-Mallah, "New analytical approach to calibrate the NaI (Tl) detectors using spherical radioactive sources," *Radiation Protection Dosimetry*, vol. 156, no. 1, pp. 109–117, 2013.
[29] M. S. Badawi, A. M. El-Khatib, and M. E. Krar, "New numerical simulation approach to calibrate the NaI(Tl) detectors array using non-axial extended spherical sources," *Journal of Instrumentation*, vol. 8, no. 11, Article ID P11005, 2013.
[30] M. M. Gouda, M. S. Badawi, A. M. El-Khatib, M. Mohamed, A. Thabet, and M. Abbas, "Calibration of well-type NaI(Tl) detector using a point sources measured out the detector well at different axial distances," *Journal of Instrumentation*, vol. 10, no. 03, Article ID P03022, 2015.
[31] M. M. Gouda, A. Hamzawy, M. S. Badawi, A. M. El-Khatib, A. A. Thabet, and M. I. Abbas, "Mathematical method to calculate full energy peak efficiency of detectors based on transfer technique," *Indian Journal of Physics*, vol. 90, no. 2, pp. 201–210, 2016.
[32] M. S. Badawi, M. Abd-Elzaher, A. A. Thabet, and A. M. El-khatib, "An empirical formula to calculate the full energy peak efficiency of scintillation detectors," *Applied Radiation and Isotopes*, vol. 74, pp. 46–49, 2013.
[33] A. A. Thabet and M. S. Badawi, "Analytical-numerical formula for estimating the characteristics of a cylindrical NaI(Tl) gamma-ray detector with a side-through hole," *Nuclear Engineering and Technology*, vol. 54, no. 10, pp. 3795–3802, 2022.
[34] M. S. Badawi, S. Noureddine, Y. N. Kopatch et al., "Characterization of the efficiency of a cubic NaI detector with rectangular cavity for axially positioned sources," *Journal of Instrumentation*, vol. 15, no. 02, Article ID P02013, 2020.
[35] M. S. Badawi, M. M. Gouda, S. S. Nafee, A. M. El-Khatib, and E. A. El-Mallah, "New analytical approach to calibrate the Coaxial HPGe detectors including correction for source matrix self-attenuation," *Applied Radiation and Isotopes*, vol. 70, no. 12, pp. 2661–2668, 2012.
[36] M. S. Badawi and A. A. Thabet, "Calibration of cylindrical NaI(Tl) gamma-ray detector intended for truncated conical radioactive source," *Nuclear Engineering and Technology*, vol. 54, no. 4, pp. 1421–1430, 2022.
[37] M. I. Abbas, M. S. Badawi, A. A. Thabet et al., "Efficiency of a cubic NaI(Tl) detector with rectangular cavity using standard radioactive point sources placed at non-axial position," *Applied Radiation and Isotopes*, vol. 163, Article ID 109139, 2020.
[38] T. Whyntie and B. Parker, "Investigating the inverse square law with the timepix hybrid silicon pixel detector: a CERN@ school demonstration experiment," *Physics Education*, vol. 48, no. 3, pp. 344–349, 2013.
[39] C. E. Gutiérrez and Ahmad Sabra, "The reflector problem and the inverse square law," *Nonlinear Analysis*, vol. 96, pp. 109–133, 2014.
[40] N. Voudoukis and S. Oikonomidis, "Inverse square law for light and radiation: a unifying educational approach," *European Journal of Engineering and Technology Research*, vol. 2, no. 11, pp. 23–27, 2017.